

## **Design of an electrically actuated lower extremity exoskeleton**

ADAM ZOSS and H. KAZEROONI\*

*Department of Mechanical Engineering, University of California, Berkeley, CA 94720, USA*

Received 13 September 2005; accepted 27 March 2006

**Abstract**—Human exoskeletons add the strength and endurance of robotics to a human’s innate intellect and adaptability to help people transport heavy loads over rough, unpredictable terrain. The Berkeley lower extremity exoskeleton (BLEEX) is the first human exoskeleton that was successfully demonstrated to walk energetically autonomous while supporting its own weight plus an external payload. This paper details the design of the electric motor actuation for BLEEX and compares it to the previously designed hydraulic actuation scheme. Clinical gait analysis data was used to approximate the torques, angles and powers required at the exoskeleton’s leg joints. Appropriately sized motors and gearing are selected, and put through a thorough power analysis. The compact electric joint design is described and the final electric joint performance is compared with BLEEX’s previous hydraulic actuation. Overall, the electric actuation scheme is about twice as efficient and twice as heavy as the hydraulic actuation.

*Keywords:* Exoskeleton; robotics; biomechanics; electric motor; actuation.

### **1. INTRODUCTION**

Although wheels are useful for moving heavy loads over flat surfaces, legged locomotion has many advantages on rough and unpredictable terrain. Legs can adapt to a wide variety of environments, such as rocky slopes and staircases, which are impassable by wheeled vehicles. However, legged robots have difficulty balancing and navigating while maneuvering through the inherently rough terrains that favor legs over wheels. Lower extremity exoskeletons seek to bypass these problems by closely integrating a human’s intelligence and adaptability with the strength and endurance of robotic legs.

Berkeley’s lower extremity exoskeleton (BLEEX) is comprised of two actuated anthropomorphic robotic legs that a person ‘wears’ (Fig. 1). As the person moves

---

\*To whom correspondence should be addressed. E-mail: [kazerooni@berkeley.edu](mailto:kazerooni@berkeley.edu)

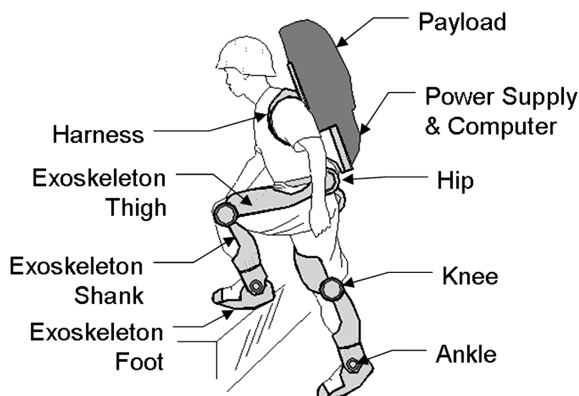


**Figure 1.** Conceptual sketch of a lower extremity human exoskeleton.

through any maneuver, the exoskeleton legs support the backpack payload mounted to the exoskeleton's torso without the person actively 'driving' the system. Thus, BLEEX provides the operator with load-carrying capability and endurance through versatile legged locomotion. BLEEX is the first energetically autonomous robotic exoskeleton that was successfully demonstrated to provide the operator with the ability to carry significant loads with minimal effort over any type of terrain. This is accomplished through four critical features: a novel control scheme, high-powered compact power supplies, special communication protocol and electronics, and a design architecture to decrease the complexity and power consumption. This paper focuses on the actuation design of the electrically actuated BLEEX.

Possible applications include helping soldiers, disaster relief workers, wildfire fighters and other emergency personnel to carry major loads without the strain typically associated with demanding labor.

## 2. BACKGROUND

Even though the field of robotics, and even humanoid robotics, has a history of successful projects, there have been relatively few attempts at powered exoskeletons and even fewer that have been demonstrated to work [1]. The first active exoskeletons were at General Electric (GE) and the Mihajlo Pupin Institute in the late 1960s and early 1970s. The Hardiman project [2] was a large, full-body exoskeleton, but safety concerns and complexity issues prevented it from ever walking. The Mihajlo Pupin lower extremity exoskeleton was designed to help rehabilitate paraplegics [3], but it only followed pre-programmed walking motions, which limited its usefulness. Neither exoskeleton could carry its own power source and operate autonomously. In the mid-1980s, Kazerooni initiated several research projects on upper extremity exoskeleton systems, billed as 'human extenders' [4–6]. The main function of an upper extremity exoskeleton is human power augmentation for manipulation of

heavy and bulky objects. These systems, which are also known as assist devices or human power extenders, can simulate forces on a worker's arms and torso.

In Japan, the Kanagawa Institute of Technology has demonstrated a full-body 'wearable power suit', powered by unique pneumatic actuators [7]. The actuation forces are controlled by measuring the hardness of the corresponding human muscles, but it lacks of a portable power supply. Tsukuba University in Japan has successfully demonstrated the lightweight power assist device, HAL [8]. Alternatively, researchers at Hokkaido University in Japan are creating a power assist device for the lower back [9]. Attached at the thigh and torso, the device uses electromyography sensors to control its electric motors.

The BLEEX project is an energetically autonomous exoskeleton capable of carrying its own weight plus an external payload. All previous exoskeletons are either tethered to a fixed power supply or not strong enough to carry an external load. BLEEX is not an orthosis or a brace; unlike the above systems, it is designed to carry a heavy load by transferring the load weight to the ground (not to the wearer). The controller controls the exoskeleton through measurements of the exoskeleton itself [10–12]. A series of high specific power and specific energy power supplies were developed that were small enough to make BLEEX a true field-operational system [13, 14].

### 3. DEGREES OF FREEDOM (d.o.f.)

To ensure maximum safety and minimum collisions with the environment and operator, the BLEEX architecture is almost anthropomorphic. This means the BLEEX leg kinematics are similar, but not identical, to the human leg kinematics. Generally, BLEEX has ankle, knee and hip joints like a person [15].

The BLEEX ankle has 3 d.o.f. just like a human ankle joint. However, only the BLEEX ankle dorsi/plantar flexion joint is aligned with the comparable human joint. BLEEX has only the flexion/extension d.o.f. at the knee joint. The human knee has movement in all 3 d.o.f., but the motion in the flexion/extension direction is the largest by far [16]. Additionally, the BLEEX knee flexion/extension joint is a rotary joint, while the human knee flexion/extension is a complex sliding and rotation between the femur and the tibia. For the hip, BLEEX has 3 d.o.f. like a human hip joint. However, like the ankle, only the BLEEX hip flexion/extension joint is aligned with the human hip. BLEEX's final d.o.f. is compliancy built into the front of the foot to yield similar flexibility to human toe joints. See Fig. 2.

### 4. CLINICAL GAIT ANALYSIS (CGA) DATA

#### 4.1. Design by biological analogy

Each BLEEX leg has 7 d.o.f. (besides the toe flexibility), but actuating all of them leads to unnecessarily high power consumption and control complexity. Instead,



**Figure 2.** Exoskeleton d.o.f.

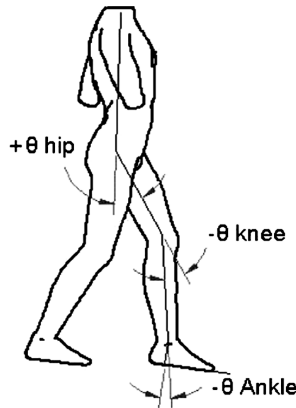


**Figure 3.** Angle and torque sign conventions. Each joint angle is measured as the positive counterclockwise displacement of the distal link from the proximal link (zero in the standing position).

only joints that require substantial power should be actuated. Since BLEEX is designed with an anthropomorphic architecture, and similar limb masses and inertias to human legs, the required exoskeleton joint powers can be estimated by the joint powers of a human performing the same maneuvers.

The required human joint powers during various maneuvers were calculated from the angles and torques of human joints obtained from independent biomechanical labs in the form of CGA data. The CGA data was modified to represent a 75-kg person (the projected weight of BLEEX and its payload not including the

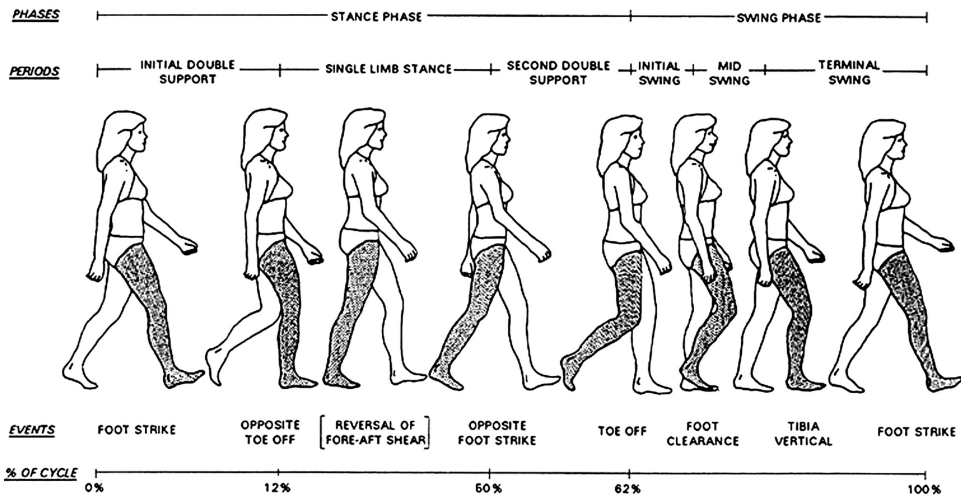


**Figure 4.** Phases of walking [16]. The walking cycle begins with the start of the stance phase (foot on the ground) at heel-strike followed by toe-off and the swing phase (foot off the ground) beginning at around 60% of the cycle.

operator). Additionally, since BLEEX has no pelvic motion, the pelvic angles (or lower back angles depending on data available) were added to the hip angles and analyzed as a single joint between the back and thigh as shown in Fig. 3. The sign conventions used in this paper (illustrated in Fig. 3) are slightly different than standard biomechanical conventions.

During the human walking cycle (shown in Fig. 4), each leg alternates between a stance phase when the foot is on the ground, supporting load and a swing phase when the foot is in the air. The leg switches from swing to stance at heel-strike (0% in Fig. 4 and subsequent plots) and it switches back to swing phase at toe-off (at around 60% of the gait cycle in Fig. 4 and subsequent plots) [16].

CGA data was analyzed for a variety of maneuvers including level ground walking, stair ascent, stair descent and inclined descent. However, for this paper, only the CGA power requirements for level ground walking at 1.3 m/s with no backpack load and stair ascent are presented.

#### 4.2. Level ground walking

The most basic requirement for any lower extremity exoskeleton is to successfully support the load during simple walking. Therefore, the joint power requirements calculated from level ground walking CGA data were heavily analyzed for the BLEEX actuation design. Given the variations in individual gait and measurement methods, three independent sources of level walking CGA data [17–19] were utilized. All of the data has been scaled for a 75-kg human walking at 1.3 m/s.

Figure 5 shows the instantaneous power required by the ankle dorsi/plantar flexion joint during level ground walking. During the first half of the stance phase the ankle

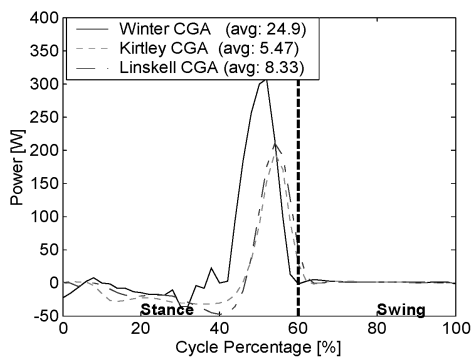


**Figure 5.** Ankle dorsi/plantar flexion powers during level walking.

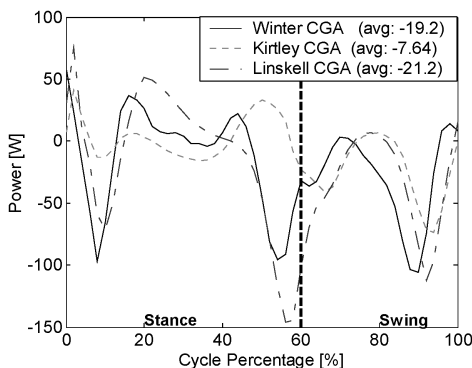


**Figure 6.** Knee flexion/extension powers during level walking.

absorbs a small amount of energy (negative power), but it requires a substantial amount of power just before toe-off. The spike in power at 50% of the gait cycle to over 200 W is the largest instantaneous power requirement of any joint during level ground walking. The ankle flexion joint also has the largest average power requirement of any joint during level ground walking, which is a strong indication that it requires actuation. During swing, the ankle powers are negligible.

The instantaneous power required by the knee flexion/extension joint is shown in Fig. 6. Since the average power is negative, the knee joint is usually dissipating power during level ground walking. The knee flexion joint dissipates by far the most power of any leg joint during level ground walking. While walking, the knee joint dynamics could closely be matched by a controlled power dissipative device (i.e., damper) as seen in many knee prosthetics.

Figure 7 shows the instantaneous hip flexion/extension power. Similar to the ankle, the hip absorbs energy during the stance phase and injects it during toe-off to propel the torso forward, but the hip power requirements are smaller than the ankle power requirements. The average power is positive, implying the need for active actuation.

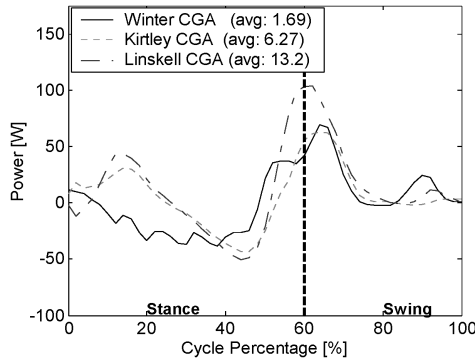


**Figure 7.** Hip flexion/extension powers during level walking.

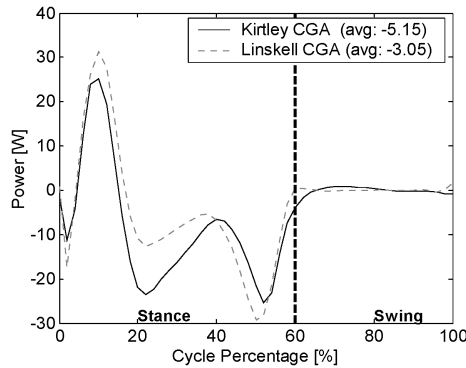


**Figure 8.** Hip abduction/adduction powers during level walking.

The instantaneous power at the hip abduction/adduction joint is illustrated in Fig. 8 for level ground walking. Critical for lateral balance of the torso, the hip abduction/adduction sees large torques, but low angular velocities and the resulting power is slightly lower than the flexion/extension joints. The power requirement is negligible during swing.

For simplicity, all of the small rotations that occur within the human leg (at the pelvis, hip, knee, shank and ankle) are summed into a net leg rotation for this paper. As seen in Fig. 9, the power requirement of the net rotation is substantially lower than the other leg joints. The net rotation power is generally always positive (consuming power) and spikes to 10–20 W near the end of the stance to correlate with the power spike in the ankle flexion. As there is so little power consumed at the rotation joints, it is probably most efficient to not actively power the leg rotation for level walking.

#### 4.3. Stair ascent

One of the most power intensive maneuvers with published biomechanical data is climbing stairs. This section describes the CGA leg flexion/extension joint powers

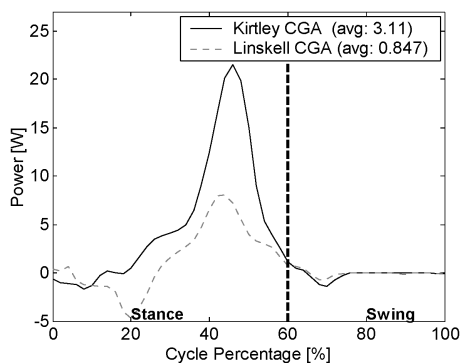


**Figure 9.** Net internal/external rotation powers during level walking.

for a human ascending various stair inclinations. The data presented here is from Riener *et al.* [20], but a more detailed three-dimensional CGA for stair ascent can be found from Duncan *et al.* [21]. During stair ascent, the ankle dorsi/plantar flexion no longer absorbs much power during the early stance (like it did during level ground walking) and it still has a large power requirement during the late stance (as seen in Fig. 10). Thus, the average ankle dorsi/plantar flexion power is slightly larger during stair ascent compared with level walking. Even during stair ascent, the ankle power is negligible during swing.

The knee flexion/extension joint shows the most dramatic change from level walking to ascending stairs (Fig. 11). The maximum instantaneous power requirement during stair ascent is 200 W compared with a 30 W maximum for level walking. Also, very little energy is absorbed at the knee during stair ascent. Thus, the average knee power is no longer negative, so the knee dynamics cannot be imitated by a controlled damper, they must be actuated to ascend stairs.

During the stance phase of stair ascent, the hip flexion/extension joint instantaneous powers are significantly more positive than during level walking (Fig. 12). However, the peak power requirement for stair ascent is the same as level walking and still occurs during the swing phase.

#### 4.4. Which d.o.f. to actuate?

It is not a power efficient actuation design to actively actuate all of the exoskeleton's degrees of freedom. Instead, the idea is to only actuate those joints that require substantial (above 10 W) positive power during the desired maneuvers. Any joints not requiring significant positive power can be moved by the human muscles with little extra effort. Since the exoskeleton's kinematics and kinetics roughly match a human's, CGA power curves (such as those presented in Sections 4.2 and 4.3) were used to estimate the required exoskeleton joint torques.

The average power the ankle uses during level walking (12.9 W) is large enough for it to require actuation, while the average hip power (7.05 W) is almost enough to require actuation. However, to successfully climb stairs, the ankle (21.4 W), knee

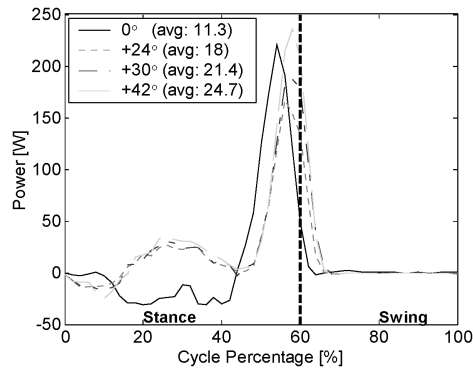


**Figure 10.** Ankle dorsi/plantar flexion powers during stair ascent.

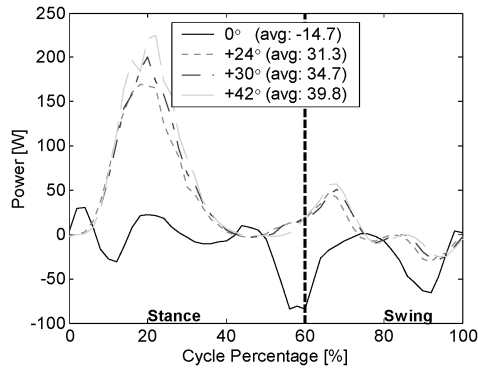


**Figure 11.** Knee flexion/extension powers during stair ascent.

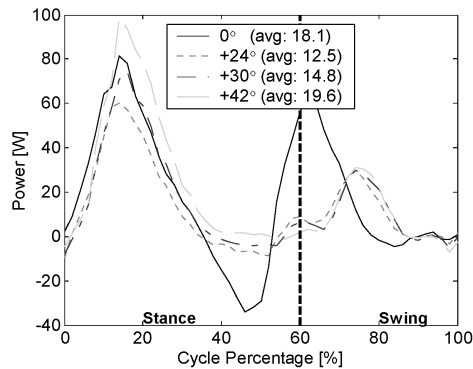


**Figure 12.** Hip flexion/extension powers during stair ascent.

(34.7 W) and hip (14.8 W) flexion joints all average large enough powers to warrant actuation. Even though it is not shown in the CGA data presented here, further exoskeleton testing resulted in adding actuation to the hip abduction/adduction joint for increased maneuverability and balance control. The unpowered d.o.f. still may

have springs, dampers or other passive elements to help remove the load from the human's leg joints. Both the powered and unpowered d.o.f. are illustrated in Fig. 2.

## 5. ELECTRIC ACTUATION SELECTION/SIZING

Two different actuation schemes have been designed to power BLEEX: hydraulic [15, 22] and electric. This paper describes the design of the electric motor actuation scheme for BLEEX and then analyzes the tradeoff of reduced power consumption, but larger size and weight, compared with hydraulic actuation.

### 5.1. Motor limit lines

*5.1.1. Winding line.* The torque,  $T$ , the motor winding can generate is proportional to the current passing through the winding,  $i$ , such that  $T = K_T i$ , where  $K_T$  is the motor's torque constant. The current in the winding during steady-state behavior is characterized by the following equation:

$$V = K_B \dot{\theta} + Ri, \quad (1)$$

where  $K_B$  is the motor's back-EMF constant,  $R$  is the motor's electrical resistance,  $\dot{\theta}$  is the motor's velocity and  $V$  is the voltage applied to the motor winding. Substituting for  $i$  in (1) results in the maximum theoretical torque from the winding of the motor,  $T_{\max}$ :

$$T_{\max} = \frac{K_T}{R} V_{\max} - K_M^2 \dot{\theta}, \quad (2)$$

where  $V_{\max}$  is the maximum available voltage to the motor and  $K_M$  is the motor constant defined as  $\sqrt{K_T K_B / R}$ . For any application, the required torque must always be less than the winding line torque (2) as shown in Fig. 13. It can be observed that the generated torque by the motor winding can be increased by either increasing the maximum voltage of the motor,  $V_{\max}$ , or selecting a thicker winding wire ( $K_T/R$  increases as the winding gets thicker). In theory,  $K_M^2$  (the slope of the winding line) does not change as one varies the motor winding.

*5.1.2. Temperature line.* The power required at the motor is determined by multiplying the motor voltage,  $V$ , by the motor current,  $i$ :

$$P = Ri^2 + T\dot{\theta} = \frac{T^2}{K_M^2} + T\dot{\theta}, \quad (3)$$

which consists of two terms: heat generated in the windings (the first term) and mechanical power (the second term). The total heat produced by the motor,  $\dot{Q}$ , is a combination of the heat from the windings plus heat generated from the motor's viscous friction:

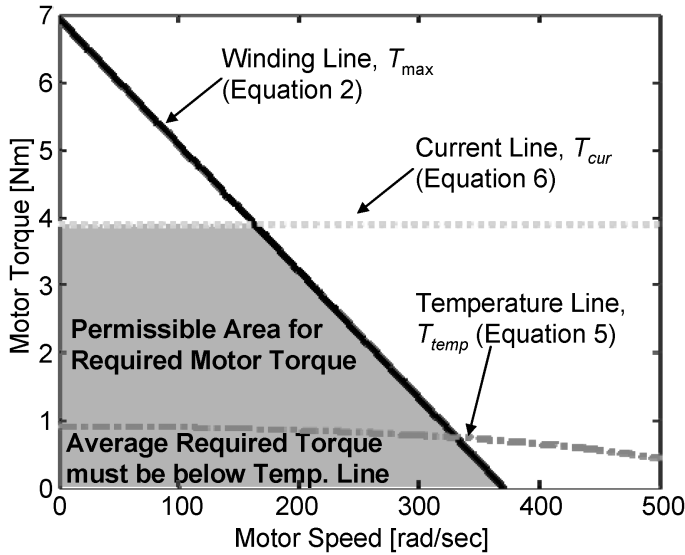


**Figure 13.** Motor limit lines for motor selection. The required motor torque must be below the winding line,  $T_{max}$ , and current limit line,  $T_{cur}$ , during all operating speeds. The average required motor torque must be below the temperature line,  $T_{temp}$ . For convenience, only the first quadrant of the motor limit lines (positive speeds and positive torques) is compared against the absolute value of the required motor torque/speed.

$$\dot{Q} = \frac{T^2}{K_M^2} + D\dot{\theta}^2, \tag{4}$$

where  $D$  is the motor’s viscous damping coefficient.

The temperature rise of the motor,  $\Delta T$ , is equal to the heat,  $\dot{Q}$ , multiplied by the motor’s thermal resistance,  $TPR$ . The maximum torque that leads to the maximum allowable temperature rise,  $\Delta T_{max}$ , is calculated by:

$$T_{temp} = K_M \sqrt{\frac{\Delta T_{max}}{TPR} - D\dot{\theta}^2}. \tag{5}$$

The average required motor torque must be smaller than the torque presented by (5) and plotted in Fig. 13. Adding external cooling to the motor or increasing the heat sink can greatly reduce  $TPR$  and thus increase the temperature line.

**5.1.3. Current limit line.** A final limit on the motor’s capabilities is either the amplifier’s maximum current or the motor’s saturation current, whichever is lower. All amplifiers have a rated maximum current before overheating or damaging their electronics. The motor has a maximum current before the steel magnetically saturates or the magnets are demagnetized. If the lowest of these current limits is  $i_{max}$ , the maximum torque the winding can produce, at any motor speed,  $T_{cur}$ , is seen in Fig. 13 and calculated by:

$$T_{cur} = K_T i_{max}. \tag{6}$$

## 5.2. Motor torque

The required motor torque must be calculated from the application and compared with the motor's winding lines (Fig. 13) to determine if the motor can produce the required joint torques. For the lower extremity human exoskeleton, the required joint torques,  $T_{\text{REQ}}$ , and speeds,  $\dot{\theta}_{\text{REQ}}$ , are the CGA torques and speeds discussed in Section 4 and found in Refs [17–19]. With a gear ratio,  $N$ , motor and gearing rotational inertia,  $I$ , and viscous damping,  $D$ , the required motor torques,  $T$ , is given by:

$$T = \frac{T_{\text{REQ}}}{N} + IN\ddot{\theta}_{\text{REQ}} + DN\dot{\theta}_{\text{REQ}}, \quad (7)$$

where  $T_{\text{REQ}}$  and  $\dot{\theta}_{\text{REQ}}$  are the required torques and speeds that form the plots of required power in Figs 5–7.

Equation (7) does not include the gearing and amplifier inefficiencies. These must be included to yield realistic torque and power calculations. Harmonic drives were selected to provide the gear ratio in the electric actuation system (Section 7.1), so the inefficiencies discussed specifically apply to harmonic drives.

- (i) Harmonic drive efficiency,  $\eta$ . Since harmonic drives require deformation of the cup to turn and create the gearing, they have relatively low efficiencies compared with planetary gears. The harmonic drive efficiency,  $\eta$ , always increases the amount of power required by the motor.

$$T = \begin{cases} \frac{T_{\text{REQ}}}{N\eta} + IN\ddot{\theta}_{\text{REQ}} + DN\dot{\theta}_{\text{REQ}} & \text{if } P \geq 0 \\ \frac{T_{\text{REQ}}\eta}{N} + IN\ddot{\theta}_{\text{REQ}} + DN\dot{\theta}_{\text{REQ}} & \text{if } P < 0. \end{cases} \quad (8)$$

- (ii) Harmonic drive no-load running torque,  $T_{\text{NL}}$ . A minimum amount of torque is required to overcome friction and turn the gears even when there is no output torque. As a conservative estimate, the torque to overcome the static friction,  $T_{\text{NL}}$ , is assumed to be the minimum torque required to move the gearing at any speed. Therefore, when the system is being back-driven, the magnitude of  $T_{\text{REQ}}$  is reduced by  $T_{\text{NL}}$ ; when the system is forward-driven, the magnitude of  $T_{\text{REQ}}$  must always be at least  $T_{\text{NL}}$ .
- (iii) Amplifier efficiencies,  $\gamma$ . All of the electric power for the motor passes through an amplifier. This amplifier has inefficiencies,  $\gamma$ , which effect the overall power consumption of the joint.

$$P = \begin{cases} \frac{T^2}{K_M^2\gamma} + TN\dot{\theta}_{\text{REQ}} & \text{if } P \geq 0 \\ \frac{T^2\gamma}{K_M^2} + TN\dot{\theta}_{\text{REQ}} & \text{if } P < 0. \end{cases} \quad (9)$$

### 5.3. Exoskeleton motor selection

The objective is to find the smallest motor that can successfully provide the motor torques given by (8). A motor and gearing combination is successful if the required torque (8) falls below the motor's winding and current limit lines ((2) and Fig. 13); further the average required torque (i.e., average torque over a cycle from (8)) must be below the motor's temperature line ((5) and Fig. 13). The required motor torque for BLEEX's joints, using (8), are calculated and plotted in Figs 14–16 for level ground walking. As seen, the most limiting factor in the motor selection is heat dissipation. Smaller motors could produce the required torques, but would generate significantly more heat and reach much larger motor temperatures. Using a bus voltage of 144 V, the electric motors selected to power the flexion joints of BLEEX are parameterized in Table 1.

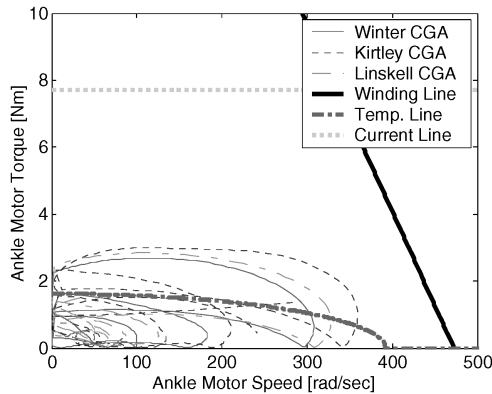


**Figure 14.** The required motor torque for the ankle as calculated from the CGA torques for level walking and using (8) should be less than the winding and current lines.

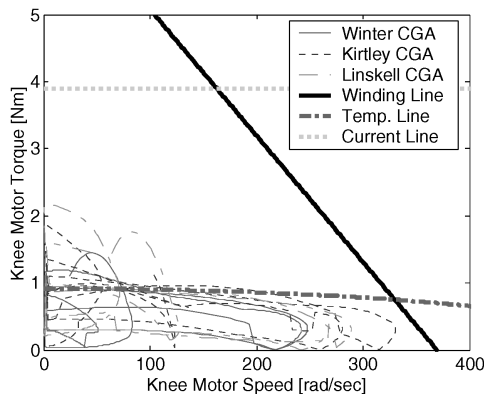


**Figure 15.** The required motor torque for the knee as calculated from the CGA torques for level walking and using (8) should be less than the winding and current lines.

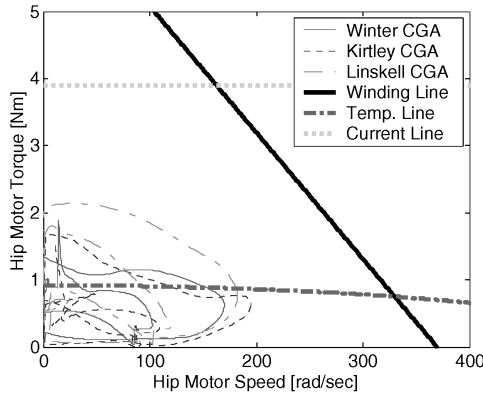


**Figure 16.** The required motor torque for the hip as calculated from the CGA torques for level walking and using (8) should be less than the winding and current lines.

**Table 1.**  
Electric motors selected for BLEEX

	Ankle	Knee	Hip	
Motor constant, $K_M$	0.237	0.138	0.138	N m/ $\sqrt{W}$
Back-EMF constant, $K_B$	31.9	40.8	40.8	V/r.p.m.
Torque constant, $K_T$	0.305	0.389	0.389	N m/A
Motor resistance, $R$	1.66	8.05	8.05	$\Omega$
Transmission ratio, $N$	80	50	50	

**6. POWER ANALYSIS**

This section examines the electric actuation power efficiency in detail and outlines the various areas of power loss. A careful analysis of the power dissipation is helpful in selecting the most power efficient motor/gearing combination and estimating the efficiency of the electric actuation.

To analyze the power losses throughout the system, the required powers were calculated at each level where inefficiencies were added into the model. As a starting reference, the desired mechanical power at the joint is calculated by:

$$P_{des} = T_{des}\dot{\theta}_{des}. \tag{10}$$

From the desired mechanical joint power additional power is consumed by the harmonic drive friction described in Section 5.2. Also included in the friction losses is the torque to overcome the motor’s viscous friction which leads to extra power equal to  $D\dot{\theta}^2$ . Also, the torque used to accelerate the motor and gearing’s rotational inertias consumes power equal to  $I\dot{\theta}\ddot{\theta}$ . Finally,  $T^2/K_M^2$  watts of power are lost in heat generated by the resistance of the motor’s windings. The estimated power losses at the electrically actuated joints during level ground walking at 1.3 m/s in Figs 17–19 (the plots go from heel-strike to subsequent heel-strike). For these plots, the solid line shows the desired mechanical joint power and the dashed

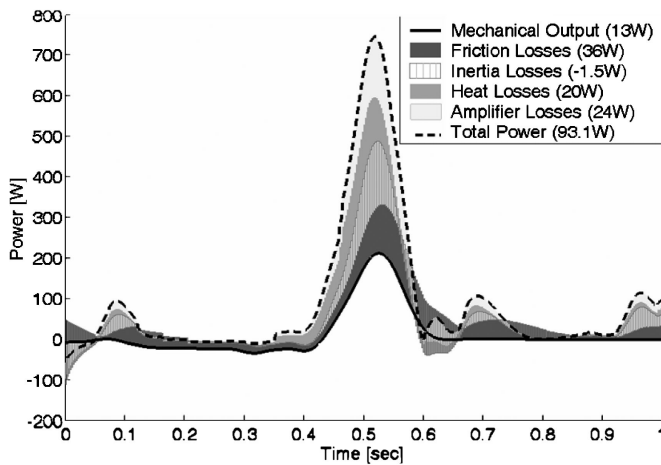


**Figure 17.** Power consumption at the ankle during level walking. The ankle requires 93 W of electrical power to produce the 13.5 W of mechanical output during level walking.

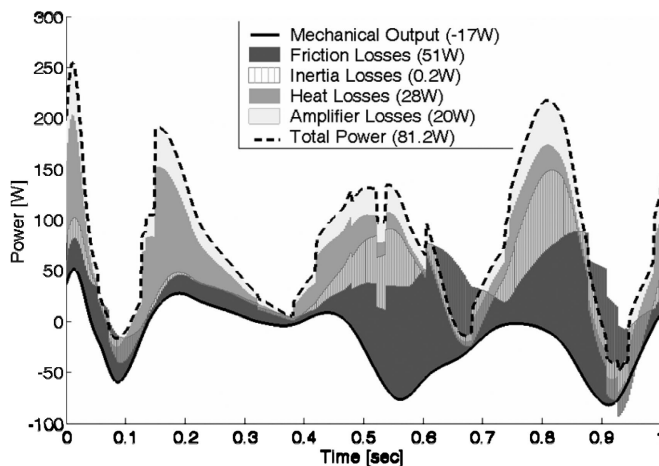


**Figure 18.** Power consumption at the knee during level walking. The knee requires 81 W of electrical power during level walking even though the joint needs to absorb 17 W of mechanical power. Gear friction is the major inefficiency at the knee joint.

line illustrates the total electrical power required to produce that desired power. The shaded areas between these two illustrate the various power losses expected from the electrical joint.

The estimated ankle power losses are shown in Fig. 17. Overall, the joint is 15% efficient, requiring 93 W to produce 13.5 W of mechanical output. The ankle shows fairly equal amounts of power dissipated by gearing friction, motor inertia, heat and the amplifier during its large power spike in the late stance.

The estimated knee power losses are shown in Fig. 18. The required knee joint power, as measured from the CGA data, is unique because it is usually dissipating

(negative) power. The torques during stance are generally large, which creates big heat losses, but when the knee is being back-driven the stance torques are large enough to back-drive the harmonic drive and turn the electric motor into a generator producing power. However, during swing, the torques are less than  $T_{NL}$ , so the power is lost in back-drive friction and then additional power is necessary to actually turn the joint. This leads to large inertial losses and friction losses during the swing phase. While the mechanical output required is  $-17$  W, the electric joint requires an estimated 81 W of power to perform the walking motion.

The estimated hip power losses are shown in Fig. 19. Overall, the estimated hip efficiency is 9.5%. Friction losses and heat losses dominate the power consumption of the hip during level ground walking.

A summary of the power requirements for the selected electric actuators during level walking at 1.3 m/s is shown in Table 2.

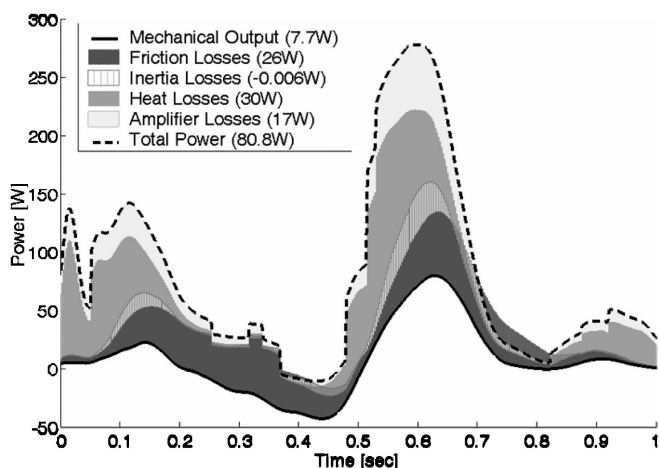


**Figure 19.** Power consumption at the hip during level walking. The hip requires 81 W of electrical power to create the 7.7 W of mechanical output power during level walking.

**Table 2.**

Electric joint power consumption

	Ankle	Knee	Hip
Power efficiency (%)	14.5	-21.2	9.5
Total motor power (W)	93.1	81.2	80.8
Output power (W)	13.5	-17.2	7.7
Heat generated (W)	25.0	30.5	31.0
Average exoskeleton power consumption: 510 W			

## 7. ELECTRIC JOINT HARDWARE

The main advantage of electrical actuation over hydraulic actuation is the increased power efficiency, but the main disadvantage is the increased size and weight of the actuated joints. Therefore, how much electric actuation is preferred to hydraulic actuation is directly impacted by how small and lightweight the electrically powered joints can be designed. Figure 20 illustrates the final electric joint hardware design and the following sections discuss details of this design.

### 7.1. Electric motor and gearing

Minimizing the joint width heavily guided the motor and gearing selection. The selected motors are ‘pancake’ style (relatively large diameter and small width), and have separate rotor and stator components (instead of being preassembled). With just the bare rotor and stator, the motor can be tightly integrated into the mechanical structure of the joint; however, the design must meet the required mounting tolerances, provide the necessary bearings and sufficiently extract heat from the motor.

The large torques seen at the joints and large desired gear ratios eliminated some gear options, and other options were eliminated because they would create too large of a joint. Harmonic drives were selected because of their large torque capacities, high gear ratios and small size. HD System’s CSD harmonic drives were specifically chosen because they have the smallest width of any available harmonic drive and, like the motors, are available as components which can be closely integrated into the mechanical structure.

### 7.2. Joint sensors

Incorporating the joint angle and torque measurements, without significantly affecting the overall joint width, proved to be one of the largest design challenges.

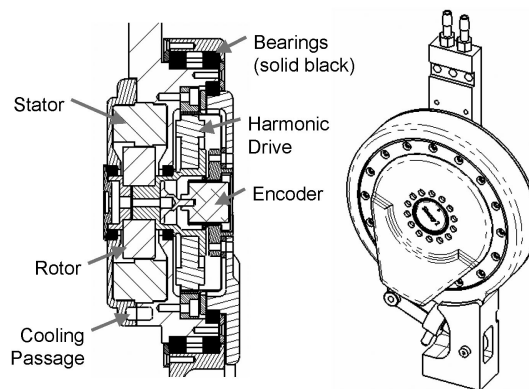


**Figure 20.** Electric joint hardware design.

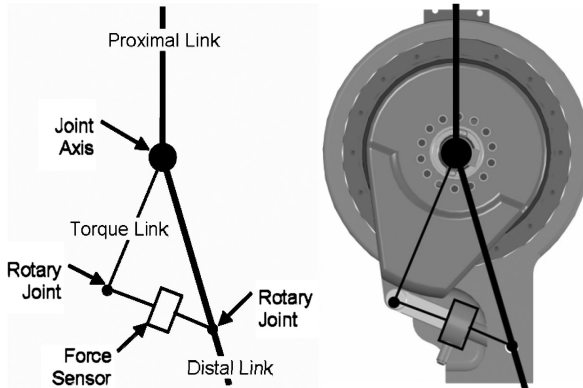


**Figure 21.** Torque sensing using a force sensor.

Miniature rotary optical encoders are placed inside the harmonic drive (see Fig. 20) to measure motor shaft angle (from which the joint angle can be calculated).

After thorough searching, even the smallest available custom torque sensors increase the overall joint width by at least 30% (or 1.91 cm). Thus, a novel technique was created to produce a torque sensor using a small, compact force sensor. Instead of creating a torque directly between the joint's proximal and distal links, the harmonic drive creates a torque between the proximal link and a third, torque, link (seen in Fig. 21). A force sensor is then placed between the torque link and the distal link. Since the torque link and distal link both pivot about the joint axis, the force sensor rigidly connects the two together. By attaching the force sensor with rotary joints, it is not subjected to any bending moments. Thus, the force sensor measures the joint torque without increasing the overall joint width.

### 7.3. Bearings

To support the rotating components of the electric joint, there are three groups of bearings (seen in solid black in Fig. 20):

- (i) Main joint bearings. These bearings provide the relative rotation between the joint's proximal and distal links. They support significant off-axis moments, but operate at very low speeds. Two angular contact bearings create a compact, high-moment-capacity bearing set. Since they are constrained as a pair, the races of an identical bearing provide a very precise spacer to prevent uneven loading of the two bearings.
- (ii) Motor shaft bearings. While these bearings do not see much loading, they need to operate at high speeds.
- (iii) Torque link bearings. Due to the unique torque sensing method implemented (Fig. 21) the additional torque link also needs to be supported on bearings. This link is low speed and does not see any large off-axis moments; therefore, a single X-contact bearing supports the torque link.

**Table 3.**  
Electric joint cooling performance for level walking

	Ankle	Knee	Hip
Motor temperature ( $^{\circ}\text{C}$ )	50	52	52.5
Motor heat removed (W)	25.7	30.6	31.9
Amplifier temperature ( $^{\circ}\text{C}$ )	48	47	47
Amplifier heat removed (W)	13.7	11.7	11.6
Total heat removed: 250 W			

#### 7.4. Electric joint cooling

The torque capability of the motors is greatly increased if they are prevented from overheating and Figs 14–16 illustrate how the selected motors are temperature limited even during level walking. Therefore, the electric exoskeleton joints are designed to be cooled via a liquid cooling channel built into the mechanical structure as close as possible to the motor stator's steel structure. When necessary, coolant is pumped into each joint, around the hot motor and then up to a radiator to cool it back down. All six of the exoskeleton's flexion joints can be significantly cooled by a relatively small 15 W/ $^{\circ}\text{C}$  radiator. The coolant is also used to remove heat generated by the amplifiers.

To help determine the overall system capabilities, the cooling performance was modeled using basic heat transfer equations. The heat generated during level walking (found in Table 2) can be fully removed by the coolant if the motors surface temperatures reach the values found in Table 3. With the liquid cooling, the motor temperatures only reach 50 $^{\circ}\text{C}$ , leaving significant room for more heat dissipation during more aggressive maneuvers before the 95 $^{\circ}\text{C}$  limit from the manufacturers is reached.

## 8. EXPERIMENTAL PROTOTYPE

A prototype electrically actuated joint is shown in Fig. 22. The joints have a 15.56 cm outer diameter and its width is 6.45 cm. Overall, the electric joint weighs an average of 4.1 kg. Generally, this is about twice as heavy as the hydraulic joints. Also the electric joint weight is all centered at the actual joint, while the hydraulic joints have about 40% of their weight (manifold, fittings, valve) located away from the joint's axis of revolution. Table 4 gives a comparison of the joint weight and power consumption during level ground walking at 1.3 m/s between the electrically and hydraulically actuated joint designs. The electric joint is about 95% heavier and 92% more power efficient during level walking.

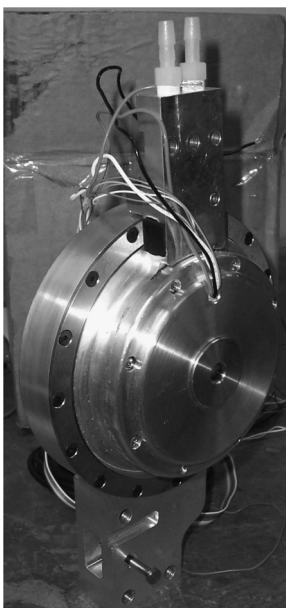


**Figure 22.** Electric joint prototype.

**Table 4.**  
Hydraulic and electric actuation comparison

	Electric actuation	Hydraulic actuation
Joint weight (kg)	4.1	2.1
Level walking power consumption (W)	598	1145

## 9. CONCLUSIONS

This paper has presented a method for selecting appropriate sized electric actuators and gearing to power the sagittal plane joints of a human exoskeleton. Fully detailed motor torque versus speed curves were derived and compared with the motor's capabilities to determine the proper motor size. Due to the difficulty in determining the desired joint torque/speed curves, CGA data was used as a first-order estimate of the exoskeleton joint requirements. Finally, a thorough power analysis was performed to determine which inefficiencies were driving the electric actuation selection.

While it was previously known that there would be a tradeoff between increasing system efficiency and increasing actuation size and weight, this work has specifically quantified the size of the tradeoff for a lower extremity exoskeleton. Even though the electric joints are substantially heavier, their significant reduction in power consumption while walking is too important to ignore. The biggest concern about the larger electric actuation size is that it is located down on the legs (especially at the ankle) and, therefore, leads to larger torque requirements during

swing. If the same power efficient motor scheme could be used, but the bulk of the weight moved up towards the torso, then the electric actuation scheme would be significantly more desirable.

### Acknowledgements

This work is partially funded by DARPA grant DAAD19-01-1-0509.

### REFERENCES

1. Y. Hurmuzlu and O. Nwokah, *The Mechanical Systems Design Handbook*. CRC Press, Boca Raton, FL (2002).
2. B. J. Makinson, General Electric Co., Research and development prototype for machine augmentation of human strength and endurance, Hardiman I project, *General Electric Report S-71-1056*, Schenectady, NY (1971).
3. M. Vukobratovic, D. Hristic and Z. Stojiljkovic, Development of active anthropomorphic exoskeletons, *Med. Biol. Eng.* **20**, 66–80 (1974).
4. H. Kazerooni and J. Guo, Human extenders, *ASME J. Dyn. Syst. Meas. Control* **115** (1993).
5. H. Kazerooni, Human–robot interaction via the transfer of power and information signals, *IEEE Trans. Syst. Cybernet.* **20**, 450–463 (1990).
6. H. Kazerooni, The human power amplifier technology at the University of California, Berkeley, *J. Robotics Autonomous Syst.* **19**, 179–187 (1996).
7. K. Yamamoto, K. Hyodo, M. Ishii and T. Matsuo, Development of power assisting suit for assisting nurse labor, *JSME Int. J. Ser. C* **45**, 703–711 (2002).
8. H. Kawamoto and Y. Sankai, Power assist system HAL-3 for gait disorder person, in: *Proc. 8th Int. Conf. on Computers Helping People with Special Needs*, Berlin (2002).
9. K. Naruse, S. Kawai, H. Yokoi and Y. Kakazu, Design of compact and lightweight wearable power assist device, in: *Proc. ASME Int. Mechanical Engineering Congr. and Exp.*, Washington, DC, pp. 525–532 (2003).
10. H. Kazerooni and R. Steger, The Berkeley lower extremity exoskeleton, *ASME J. Dyn. Syst. Meas. Control* **128**, 14–25 (2006).
11. H. Kazerooni, L. Huang and R. Steger, On the control of the Berkeley Lower Extremity Exoskeleton (BLEEX), in: *Proc. IEEE Int. Conf. on Robotics and Automation*, Barcelona, pp. 4353–4360 (2005).
12. S. Kim, G. Anwar and H. Kazerooni, High-speed communication network for controls with application on the exoskeleton, in: *Proc. Am. Control Conf.*, Boston, MA, pp. 355–360 (2004).
13. J. Raade, H. Kazerooni and T. McGee, Analysis and design of a novel power supply for Mobile robots, *IEEE Trans. Automat. Sci. Eng.* **2**, 226–232 (2005).
14. K. Amundson, J. Raade, N. Harding and H. Kazerooni, Hybrid hydraulic–electric power unit for field and service robots, in: *Proc. IEEE Int. Conf. on Intelligent Robots and Systems*, Edmonton, pp. 3453–3458 (2005).
15. A. Chu, H. Kazerooni and A. Zoss, On the biomimetic design of the Berkeley lower extremity exoskeleton (BLEEX), in: *Proc. IEEE Int. Conf. on Robotics and Automation*, Barcelona, pp. 4345–4352 (2005).
16. J. Rose and J. G. Gamble, *Human Walking*, 2nd edn. Williams & Wilkins, Baltimore, MD (1994).
17. C. Kirtley, CGA Normative Gait Database, Hong Kong Polytechnic University. Available: <http://guardian.curtin.edu.au/cga/data/> (2006).
18. D. A. Winter, International Society of Biomechanics, Biomechanical Data Resources, Gait Data. Available: <http://www.isbweb.org/data/> (2006).

19. J. Linsell, CGA Normative Gait Database, Limb Fitting Centre, Dundee. Available: <http://guardian.curtin.edu.au/cga/data/> (2006).
20. R. Riener, M. Rabuffetti and C. Frigo, Stair ascent and descent at different inclinations, *Gait and Posture* **15**, 32–34 (2002).
21. J. A. Duncan, D. L. Kowalk and C. H. Vaughan, Six degree of freedom joint power in stair climbing, *Gait and Posture* **5**, 204–210 (1997).
22. A. Zoss, H. Kazerooni and A. Chu, Biomimetic design of a lower extremity exoskeleton, *ASME/IEEE Trans. Mechatron.* **11**, 128–138 (2006).

## ABOUT THE AUTHORS



**Adam Zoss** received his BS degree from the University of Texas, Austin and his MS degree from the University of California, Berkeley, both in Mechanical Engineering. He is currently a PhD candidate in the Robotics and Human Engineering Laboratory at the University of California, Berkeley researching robotics and mechatronics.



**H. Kazerooni** received the MS and PhD degrees in Mechanical Engineering from the Massachusetts Institute of Technology, Cambridge, in 1982 and 1984, respectively. He is currently a Professor in the Mechanical Engineering Department at the University of California, Berkeley, and Director of the Berkeley Robotics and Human Engineering Laboratory.